I. Troch, F. Breitenecker, eds. ISBN 978-3-901608-35-3

CONTROL OF FLEXIBLE VIBRATIONS IN A TWO-LINK ROBOT BY PIEZOELECTRIC ACTUATION

C. Zehetner[1], J. Gerstmayr[2]
[1,2]Linz Center of Mechatronics, Linz, Austria

Corresponding author: C. Zehetner, Linz Center of Mechatronics GmbH, Altenbergerstr. 69, A-4040 Linz, Austria; christian.zehetner@lcm.at

Abstract. This paper concerns the active control of flexural vibrations in a two-link robot consisting of two flexible arms with tip masses. Due to inertial forces of distributed and concentrated masses flexural vibrations occur. The robot is moving in a horizontal plane, such that it is not necessary to consider gravity. In order to compensate the flexible vibrations, piezoelectric actuators are integrated in the arms. In the first step a shape control solution is presented in the framework of linear beam theory: Assuming that the angles of the two links are known by appropriate measurements, the necessary distribution of piezoelectric actuation is derived in order to compensate the flexible vibrations. This solution represents a feed-forward control strategy. In the second step, it is assumed that masses and geometrical parameters are not exactly known, and that the distribution of actuation strains is approximated by the use of a limited number of piezoelectric patches. In order to reduce the remaining flexible vibrations, an additional PD controller is employed for the piezoelectric actuated patches. The proportional (P) part of the controller keeps the curvature, measured by sensor patches, near the value given by the optimal distribution of the patches. The differential (D) part of the controller aims to damp the remaining vibrations of the beam. A numerical example of a highly flexible robot with three patches per arm is studied. The robot shows significantly reduced vibrations and the control scheme turns out to be robust with respect to variation of system parameters.

1 Introduction

The present paper deals with the control of vibrations in flexible multi-body systems using piezoelectric patch sensors and actuators [1]. Exemplarily, a two-link robot consisting of two flexible arms with concentrated tip masses is considered, in which flexible vibrations are caused by inertial forces. In the first step, a solution of the shape control problem is applied, i.e. the distribution of piezoelectric actuation strains is derived in order to compensate the inertial forces. For review on shape control of structures see Irschik [2], applications to elastic structures performing large rigidbody motions have been presented in [3] - [5].

The shape control solution can be considered as a feed-forward control strategy: Assuming that the inertial forces are known by appropriate measurement of the link angles and their time-derivatives, the distributed actuating moment is applied by piezoelectric actuation. It turns out that for each arm at least three spatially distributed actuating moments with different time responses are needed in order to completely compensate the inertial forces. With regard to practical applications, the distributed actuation is realized by a limited number of piezoelectric patches. Earlier investigations showed that the replacement of the shaped actuator layers by means of rectangular actuator patches leads to a system which can compensate the vibrations, and stable control algorithms can be implemented, see Krommer and Irschik [6] and Nader et al. [7].

In the second step, it is assumed that mass-distribution and geometrical properties of the robot are not exactly known and that the realization of the actuating moment by piezoelectric patches is an approximation of the exact solution. Thus, it is not possible, to completely compensate the flexible vibrations with the help of feed-forward shape control. In order to minimize the remaining vibrations, an additional closed loop control algorithm is employed. Measuring the curvature of the beam with the help of piezoelectric patches, a PD-controller is added to the piezoelectric actuated patches. The proportional (P) part of the controller keeps the curvature of the beam near the value given by the optimal distribution of the patches. The differential (D) part of the controller aims to damp the vibrations of the beam. By assuming that the third time-derivative of the joint angle cannot be measured accurately, the differential part only damps out low frequency vibrations of the robot arms.

In order to investigate the behavior of the open loop and the closed loop control algorithms, a numerical model including large deformation beam elements for the robot arms, the actuating piezo elements and the open and closed loop controllers have been implemented within the multibody dynamics simulation code HOTINT (see http://tmech.mechatronik.uni-linz.ac.at/staff/gerstmayr/hotint.html). The beam elements are based on specific large deformation beam elements, which are available for the Bernoulli Euler case [8] and the shear deformable (Timoshenko) case [9]. Numerical computations are performed with main goal to find an efficient configuration of patches and to test if the system shows the desired behavior. A numerical example of a highly flexible robot with three patches per arm is studied which shows significantly reduced vibrations and turns out to be robust with respect to variation of system parameters.

2 Shape control of a moving cantilever beam

Figure 1 shows an initially straight laminated elastic beam moving in a horizontal plane. An inertial frame with the Cartesian coordinates (x_0, y_0, z_0) is introduced, where the plane under consideration is parallel to the plane (x_0, z_0). Furthermore, a floating frame with a Cartesian coordinate-system (x, y, z) is fixed to the end B of the beam. For the notion of a floating frame of reference, see Shabana [10]. The floating coordinate system is rotated with respect to the inertial one by the angle φ about the y-axis. The x-axis of the floating system is used to define a floating straight reference configuration, represented by the dashed straight line in figure 1, with respect to which the beam performs vibrations in the (x, z) plane. For an observer co-moving with the floating frame, the beam appears to be clamped in point B, the x-axis playing the role of the beam axis. We assume the (y, z) axes to be parallel to the principal axes of inertia of the cross-sections of the beam, such that plane vibrations can take place.

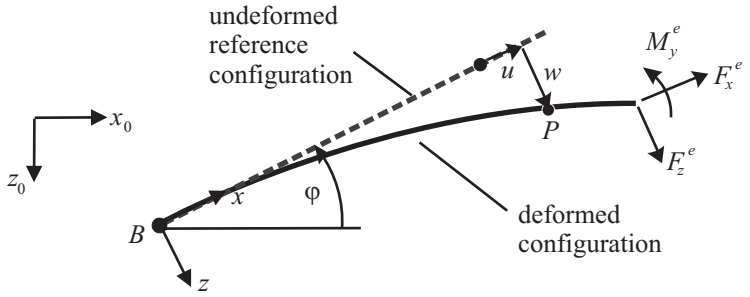

Figure 1: Kinematics of the beam

In the floating frame, the position vector $\mathbf{x}_P$ and displacement vector $\mathbf{u}_P$ of point P on the beam axis are given by

$$\mathbf{x}_P = (x+u)\mathbf{e}_x + w\mathbf{e}_y, \qquad \mathbf{u}_P = u\mathbf{e}_x + w\mathbf{e}_y, \tag{1}$$

with the axial displacement $u = u(x,t)$, the deflection $w = w(x,t)$ and the unit vectors $\mathbf{e}_x$, $\mathbf{e}_y$ and $\mathbf{e}_z$ of the floating frame of reference. The actual position of the origin B of the floating frame is given by the coordinates $x_B^0 = x_B^0(t)$ and $z_B^0 = z_B^0(t)$, where the superscript 0 indicates that the latter co-ordinates are measured in the inertial frame. The rotation of the reference frame with respect to the inertial frame is described by the angle $\varphi = \varphi(t)$. The angle φ and the coordinates x_B^0 and z_B^0 thus define the rigidbody motion of the beam. The absolut position vector (in the inertial system) thus reads

$$\mathbf{x}_P^0 = [x_B^0 + (x+u)\cos\varphi + w\sin\varphi]\mathbf{e}_x + [z_B^0 - (x+u)\sin\varphi + w\cos\varphi]\mathbf{e}_z. \tag{2}$$

The acceleration of P in the inertial frame can be obtained by differentiating eq. (2) twice with respect to time. In the following, we assume that the elastic displacements and strains are small, and that the beam is so slender, such that we can apply the Bernoulli-Euler hypotheses of cross-sections remaining plane and perpendicular to the deformed axis, which is also called a single-layer beam theory rigid in shear. The axial strain with respect to the floating frame of reference is hence written as

$$\varepsilon_{xx} = u' - zw''. \tag{3}$$

Here and in the following, a prime denotes the derivative with respect to the variable x. As external excitations, a concentrated force $\mathbf{F}_e$ and a concentrated moment $\mathbf{M}_e$ are considered as shown in Figure 1,

$$\mathbf{F}^e = F_x^e\mathbf{e}_x + F_z^e\mathbf{e}_z, \qquad \mathbf{M}^e = M_y^e\mathbf{e}_y. \tag{4}$$

In the framework of Bernoulli-Euler beam theory, axial stress is assumed to be predominant, such that the consitutive relations for a laminated beam consisting of passive and actuating layers are given in the additive form

$$\sigma_{xx} = E(\varepsilon_{xx} - \varepsilon_{xx}^0), \tag{5}$$

where σ_{xx} is the axial component of stress, E is an effective Young modulus and ε_{xx}^0 is called the axial eigenstrain. In thermoelastic materials, for example, this eigenstrain would be equal to the thermal expansion strain, $\varepsilon_{xx}^0 = \alpha(T - T_0)$, with the thermal expansion coefficient α, temperature T, and the constant reference temperature T_0. In thin piezoelectric layers, the eigenstrain

$$\varepsilon_{xx}^0 = d_{31}E_z \tag{6}$$

represents the converse piezoelectric effect, with the piezoelectric coefficient d_{31} and the electric field E_z in thickness direction of an actuating layer. Putting eq. (3) into eq. (5) and integrating over the cross-section A gives normal force N and bending moment M,

$$N = A_{11}u' - N_a, \qquad M = -D_{11}w'' - M_a, \tag{7}$$

where $A_{11} = A_{11}(x)$ is the effective extensional stiffness and $D_{11} = D_{11}(x)$ the effective bending stiffness of the laminated beam, $N_a = N_a(x,t)$ and $M_a = M_a(x,t)$ are the actuating force and moment, respectively. These quantities read

$$A_{11} = \int_A E \, \mathrm{d}A, \qquad D_{11} = \int_A E z^2 \, \mathrm{d}A, \qquad N_a = \int_A E \varepsilon_{xx}^0 \, \mathrm{d}A, \qquad M_a = \int_A E \varepsilon_{xx}^0 z \, \mathrm{d}A. \tag{8}$$

The equations of motion for the beam in Figure 1 have been derived by Zehetner and Irschik [5] considering the v.Karman part of strain. Neglecting the latter, we obtain

$$(A_{11}u')' - \mu(\ddot{u} + 2\dot{w}\dot{\varphi} + w\ddot{\varphi} - u\dot{\varphi}^2) = N_a' - q_x^e, \tag{9}$$

$$-(D_{11}w'')'' - \mu(\ddot{w} + 2\dot{u}\dot{\varphi} - u\ddot{\varphi} - w\dot{\varphi}^2) = M_a'' - q_z^e, \tag{10}$$

with the maass per unit length $\mu = \mu(x) = \int_{A(x)} \rho(x) \mathrm{d}A$ and the boundary conditions

$$x = 0 \quad : \quad u = w = w' = 0, \tag{11}$$

$$x = L \quad : \quad A_{11}u' = F_x^e + N_a, \qquad -(D_{11}w'')' = F_z^e + M_a' \qquad -D_{11}w'' = M_y^e + M_a. \tag{12}$$

In Eqs. (9) and (10), $q_x^e = q_x^e(x,t)$ and $q_z^e = q_z^e(x,t)$ are effective distributed forces per unit length,

$$q_x^e = -\mu(\ddot{x}_B^0 \cos\varphi - \ddot{z}_B^0 \sin\varphi - x\dot{\varphi}^2), \qquad q_z^e = -\mu(\ddot{x}_B^0 \sin\varphi + \ddot{z}_B^0 \cos\varphi - x\ddot{\varphi}), \tag{13}$$

The initial-boundary value problem formed by equations (9) - (12) is linear with respect to the flexible coordinates u and w. Recall that φ, x_B^0 and z_B^0 are considered as prescribed functions of time.

In the following the solution of shape control is formulated: The effective external excitations are compensated, if the right hand sides of Eqs. (9), (10) and (12) vanish, i.e.

$$0 < x < L \quad : \quad N'_a = q_x^e, \quad M_a'' = q_z^e, \tag{14}$$

$$x = L \quad : \quad N_a = -F_x^e, \quad M_a = -M_y^e, \quad M'_a = -F_z^e.$$

If the motion starts from rest, i.e. $w(t=0) = \dot{w}(t=0) = u(t=0) = \dot{u}(t=0) = 0$, then the elastic displacements vanish,

$$w(x,t) = 0, \qquad u(x,t) = 0. \tag{15}$$

Care has to be taken with respect to the fact that equation (15) may not be the only solution. E.g. a heavy beam may reach a buckled state in the course of the motion. On the other hand, the geometric stiffening effect is not accounted for in the equations of motion, such that instable solutions may occur for large angular velocities. Such effects have been studied in [5] considering the v.Karman part of strain.

In the following, it is assumed that such instabilities do not occur. Integration of Eq. (14) yields the actuating force and moment which have to be induced by the actuators in order to compensate the external excitations,

$$N_a = -F_x^e - L\int_\xi^1 q_x(\overline{\xi}) \, \mathrm{d}\overline{\xi}, \tag{16}$$

$$M_a = -M_y^e - F_z^e L(1-\xi) - L^2 \int_\xi^1 (\overline{\xi} - \xi) q_z(\overline{\xi}) \, \mathrm{d}\overline{\xi}, \qquad \xi = \mathrm{x/L}. \tag{17}$$

Assuming that all system parameters like rigidbody motion, mass distribution and geometrical properties are exactly known, the elastic deformation of the beam can be completely suppressed with the actuating normal force and bending moment in Eqs. (16) and (17). The solution of shape control can thus be interpreted as feed-forward control law. In the following section, shape control is applied to a two-link robot.

3 Compensation of flexural vibrations in a two-link robot

Figure 2 shows the investigated two-link robot consisting of two flexible arms with lengths L_1 and L_2, respectively, masses per unit length μ_1 and μ_2 and tip masses m_1 and m_2.

In the following, the axial elastic displacement u is neglected, such that shape control is only applied with respect to the deflection w, i.e. the actuating normal force is set to zero, $N_a = 0$, and the axial vibrations remain uncontrolled.

In order to derive the actuating moments $M_{a,1}$ and $M_{a,2}$ for the two arms of the robot, we have to express the effective excitations, see Figure 3. The distributed forces per unit length of arm 1 and 2, respectively, are given by

$$\begin{bmatrix} q_{x,1}^e \\ q_{z,1}^e \end{bmatrix} = \mu_1 \xi L_1 \begin{bmatrix} \dot{\varphi}_1^2 \\ \ddot{\varphi}_1 \end{bmatrix}, \qquad \begin{bmatrix} q_{x,2}^e \\ q_{z,2}^e \end{bmatrix} = \mu_2 L_1 \begin{bmatrix} g_{x,1}(t) \\ g_{z,1}(t) \end{bmatrix} + \mu_2 \xi L_2 \begin{bmatrix} g_{x,2}(t) \\ g_{z,2}(t) \end{bmatrix}, \tag{18}$$

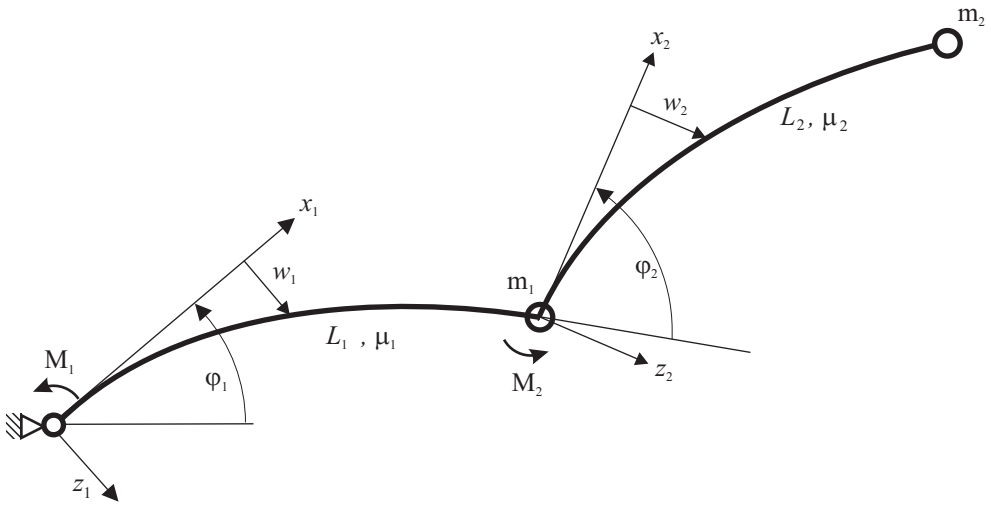

Figure 2: Two-link robot

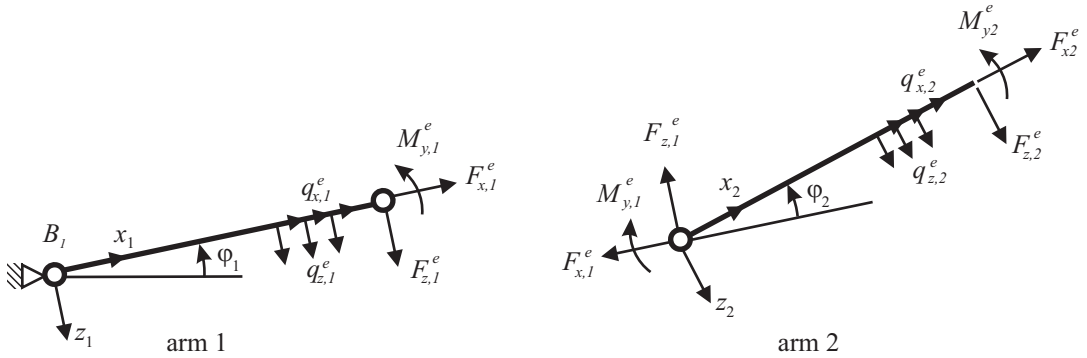

Figure 3: Effective excitations of arm 1 and 2

where $\phi_2 = \varphi_1 + \varphi_2$ has been introduced and $g_{x,1}$, $g_{z,1}$, $g_{x,2}$ and $g_{z,2}$ are functions of time,

$$\begin{aligned} g_{x,1}(t) &= \ddot{\varphi}_1(\cos\phi_2 \sin\varphi_1 - \sin\phi_2 \cos\varphi_1) + \dot{\varphi}_1^2(\cos\phi_2 cos\varphi_1 + \sin\phi_2 \sin\varphi_1), \\ g_{z,1}(t) &= \ddot{\varphi}_1(\sin\phi_2 \sin\varphi_1 + \cos\phi_2 \cos\varphi_1) + \dot{\varphi}_1^2(\sin\phi_2 cos\varphi_1 - \cos\phi_2 \sin\varphi_1), \\ g_{x,2}(t) &= \dot{\phi}_2^2, \\ g_{z,2}(t) &= \ddot{\varphi}_2. \end{aligned} \tag{19}$$

The tip forces are given by

$$\begin{aligned} \begin{bmatrix} F^e_{x,1} \\ F^e_{z,1} \end{bmatrix} &= m_1 L_1 \begin{bmatrix} \dot{\varphi}_1^2 \\ \ddot{\varphi}_1 \end{bmatrix} + m_2 \begin{bmatrix} h_{x,1}(t) \\ h_{z,1}(t) \end{bmatrix} + \mu_2 L_2 \begin{bmatrix} h_{x,2}(t) \\ h_{z,2}(t) \end{bmatrix}, \\ \begin{bmatrix} F^e_{x,2} \\ F^e_{z,2} \end{bmatrix} &= m_2 L_1 \begin{bmatrix} g_{x,1}(t) \\ g_{z,1}(t) \end{bmatrix} + m_2 L_2 \begin{bmatrix} g_{x,2}(t) \\ g_{z,2}(t) \end{bmatrix}, \end{aligned} \tag{20}$$

with the time-functions

$$\begin{aligned} h_{x,1}(t) &= (L_1 g_{x,1}(t) + L_2 g_{x,2}(t))\cos\varphi_2 + (L_1 g_{z,1}(t) + L_2 g_{z,2}(t))\sin\varphi_2, \\ h_{z,1}(t) &= -(L_1 g_{x,1}(t) + L_2 g_{x,2}(t))\sin\varphi_2 + (L_1 g_{z,1}(t) + L_2 g_{z,2}(t))\cos\varphi_2, \\ h_{x,2}(t) &= (L_1 g_{x,1}(t) + \frac{L_2}{2} g_{x,2}(t)\cos\varphi_2 + (L_1 g_{z,1}(t) + \frac{L_2}{2} g_{z,2}(t)\sin\varphi_2, \\ h_{z,2}(t) &= -(L_1 g_{x,1}(t) + \frac{L_2}{2} g_{x,2}(t)\sin\varphi_2 + (L_1 g_{z,1}(t) + \frac{L_2}{2} g_{z,2}(t)\cos\varphi_2. \end{aligned} \tag{21}$$

The tip moments read

$$\begin{aligned} M^e_{y,1} &= m_2(L_1 g_{z,1}(t) + L_2 g_{z,2}(t)) + \mu_2(\frac{1}{2} g_{z,1}(t) L_1 L_2^2 + \frac{1}{3} g_{z,2}(t) L_2^3), \\ M^e_{y,2} &= 0. \end{aligned} \tag{22}$$

With Eq. (17), the actuating moments in arm 1 and 2, respectively, follow to

$$M_{a,1} = -M^e_{y,1} - F^e_{z,1}L_1(1-\xi) - L_1^2\int_\xi^1 (\overline{\xi}-\xi)q_{z,1}(\overline{\xi})\,\mathrm{d}\overline{\xi}, \qquad \xi = x_1/L_1, \tag{23}$$

$$M_{a,2} = -F^e_{z,2}L_2(1-\xi) - L_2^2\int_\xi^1 (\overline{\xi}-\xi)q^e_{z,2}(\overline{\xi})\,\mathrm{d}\overline{\xi}, \qquad \xi = x_2/L_2.$$

Inserting Eqs. (18), (20) and (22) yields

$$\begin{aligned} M_{a,1}(\xi,t) &= \hat{M}^{(0)}_{a,1}(t)S^{(0)}(\xi) + \hat{M}^{(1)}_{a,1}(t)S^{(1)}(\xi) + \hat{M}^{(3)}_{a,1}(t)S^{(3)}(\xi), \\ M_{a,2}(\xi,t) &= \hat{M}^{(1)}_{a,2}(t)S^{(1)}(\xi) + \hat{M}^{(2)}_{a,2}(t)S^{(2)}(\xi) + \hat{M}^{(3)}_{a,2}(t)S^{(3)}(\xi), \end{aligned} \tag{24}$$

with the shape functions

$$S^{(0)}(\xi) = 1, \quad S^{(1)}(\xi) = 1-\xi, \quad S^{(2)}(\xi) = (1-\xi)^2, \quad S^{(3)}(\xi) = \frac{1}{2}(1-\xi)^2(\xi+2), \tag{25}$$

and the amplitudes

$$\begin{aligned} \hat{M}^{(0)}_{a,1}(t) &= \hat{M}^{(1)}_{a,2}(t) + \hat{M}^{(2)}_{a,2}(t) + \hat{M}^{(3)}_{a,2}(t), & \hat{M}^{(1)}_{a,2}(t) &= -m_2(L_1 g_{z,1}(t) + L_2 g_{z,2}(t)), \\ \hat{M}^{(1)}_{a,1}(t) &= L_1(m_1 L_1 \ddot{\varphi}_1 + m_2 h_{z,1}(t) + \mu_2 L_2 h_{z,2}(t)), & \hat{M}^{(2)}_{a,2}(t) &= -\frac{1}{2} g_{z,1}(t) L_1 \mu_2 L_2^2, \\ \hat{M}^{(3)}_{a,1}(t) &= \frac{1}{3}\mu_1 L_1^3 \ddot{\varphi}_1, & \hat{M}^{(3)}_{a,2}(t) &= -\frac{1}{3} g_{z,2}(t)\mu_2 L_2^3. \end{aligned} \tag{26}$$

4 Realisation with piezoelectric patches

A possible realisation of a distributed actuating moment is to mount shaped piezoelectric layers on the beam. This strategy has been investigated in [5] for a rotating flexible beam. For the investigated two-link robot three shaped piezoelectric layers would be required for each arm in order to realise the actuating moments in Eq. (24).

Using a large number of shaped piezoelectric layers is complicated and hardly practicable, such that in the following the distribution of the actuating moment is approximated by piezoelectric patches, as shown in figure 4, where l_p denotes the patch length, and l_s the length of the space between the patches.

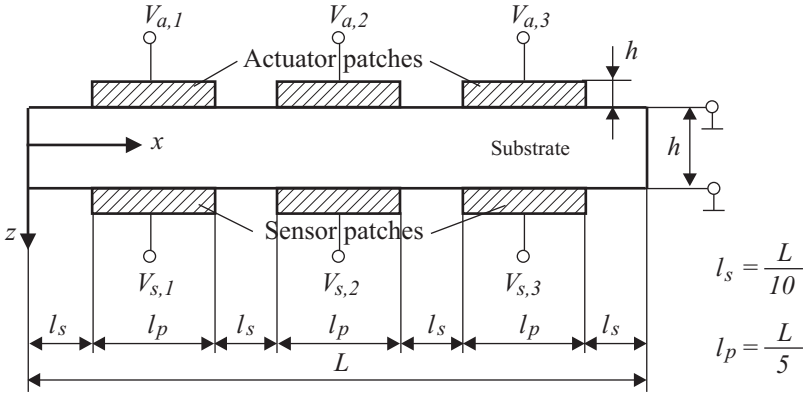

Figure 4: Realisation with piezoelectric patches

Assuming that the patches are thin, the electric field in a patch i is given by $E^i_z = V^i(t)/h_p$, with the voltage $V^i(t)$ and the patch thickness h_p. The piezoelectric eigenstrain induced by the patch follows from Eq. (6) to $\varepsilon^{0,i}_{xx} = d_{31}V^i(t)/h_p$. Inserting into Eq. (8) yields the actuating moment induced by the patch i

$$M^i_a = \frac{1}{2}E_p d_{31} b(h+h_p)V^i(t), \tag{27}$$

with the Young modulus E_p of the patch, and the beam width b. The actuating moment has a constant spatial distribution in the area of the patch.

5 Numerical modeling of the piezo-beam-element

For the numerical simulation of the piezo-electric actuated robot, a fully nonlinear beam finite element is utilized. In the following, the equations of motion of a displacement based finite element, based on the absolute nodal

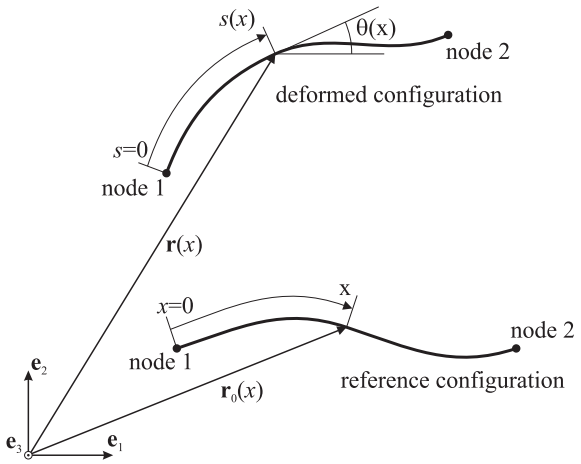

Figure 5: Planar ANCF element.

coordinate formulation (ANCF), see Shabana [10], and implemented according to Gerstmayr and Irschik [8], are presented. The beam element has been extended to a formulation based on Reissner's large deformation rod theory, see Gerstmayr et al. [9]. The planar ANCF element contains eight degrees of freedom, including coupled large bending and axial deformation. According to the Bernoulli-Euler beam theory, the latter finite element considers arbitrary large axial and bending deformation and no shear deformation. The position vector $\mathbf{r}$ of a point at the beam axis, originally placed at x, see Figure 5, is interpolated by shape functions $\mathbf{S}$ and element coordinates $\mathbf{q}$, which follows as

$$\mathbf{r} = \mathbf{S}\,\mathbf{q}, \quad \mathbf{q} = \left[\mathbf{r}^{(1)^T} \quad \mathbf{r}'^{(1)^T} \quad \mathbf{r}^{(2)^T} \quad \mathbf{r}'^{(2)^T}\right]^T \tag{28}$$

with the abbreviation $\mathbf{r}' = \frac{\partial \mathbf{r}}{\partial x}$. Here, $x \in [0,\ L]$ denotes the coordinate of the undeformed beam axis. The shape function matrix $\mathbf{S}_m$ is given as

$$\mathbf{r} = [S_1\mathbf{I} \quad S_2\mathbf{I} \quad S_3\mathbf{I} \quad S_4\mathbf{I}]\mathbf{q} = \mathbf{S}_m\mathbf{q}, \tag{29}$$

where $\mathbf{I}$ is the 2×2 unit matrix. This interpolation allows coupled bending and stretching of the beam axis, while shear is not included. The single shape functions S_i are given by

$$S_1 = 1 - 3\frac{x^2}{L^2} + 2\frac{x^3}{L^3}, \quad S_2 = x - 2\frac{x^2}{L} + \frac{x^3}{L^2}, \quad S_3 = 3\frac{x^2}{L^2} - 2\frac{x^3}{L^3}, \quad S_4 = -\frac{x^2}{L} + \frac{x^3}{L^2}. \tag{30}$$

5.1 Equations of motion

The weak form of the equations of motion is derived from the Lagrange-D'Alembert equation,

$$\delta W_I + \delta W_S - \delta W_E = 0, \tag{31}$$

in which δW_I denotes the virtual work of inertia forces, δW_S is the virtual work of internal (elastic) forces and δW_E is the virtual work of external forces. The mass matrix is determined from the kinetic energy,

$$T = \frac{1}{2}\int_L \rho A \dot{\mathbf{r}}^T \dot{\mathbf{r}}\, dx = \dot{\mathbf{q}}^T \int_0^L \rho A \mathbf{S}_m^T \mathbf{S}_m\, dx\, \dot{\mathbf{q}} = \dot{\mathbf{q}}^T \mathbf{M} \dot{\mathbf{q}} \tag{32}$$

and is defined by $\mathbf{M} = \int_0^L \rho A \mathbf{S}_m^T \mathbf{S}_m\, dx$. Here, A denotes the cross sectional area of the beam element and ρ is the density. The mass matrix is constant and can be stored in sparse form. The virtual work of inertia forces (I) and external forces (E) follow as

$$\delta W_I = \ddot{\mathbf{q}}^T \mathbf{M}\, \delta\mathbf{q} \quad \text{and} \quad \delta W_E^b = \int_L A\mathbf{b}^T \delta\mathbf{r}(x)\, dx. \tag{33}$$

The virtual work of elastic forces is defined by

$$\delta W_S = \int_0^L A_{11}(\varepsilon - \varepsilon_0)\delta\varepsilon + D_{11}(K - K_0)\delta K\, dx. \tag{34}$$

For details see the paper of Gerstmayr and Irschik [8]. The quantity K, sometimes denoted as the material measure of curvature, is defined by the rate of rotation θ of the cross section,

$$\theta' = \frac{\partial\theta}{\partial s}\frac{\partial s}{\partial x} = \kappa\frac{\partial s}{\partial x} = K = \left(\frac{\mathbf{r}' \times \mathbf{r}''}{|\mathbf{r}'|^2}\right)^T \mathbf{e}_3. \tag{35}$$

The axial strain in the Bernoulli-Euler beam can be split into normal and bending strain, respectively,

$$\varepsilon = |\mathbf{r}'| - 1 \quad \text{and} \quad \varepsilon_{bend} = yK. \tag{36}$$

Eigenstrains are considered by means of the normal strain ε_0 and the bending strain K_0. The latter two quantities are utilized to include piezo-electric actuation in the large deformation beam element. The terms ε_0 and K_0 are equivalent to initial stretch and initial curvature in a pre-curved beam element. The piezo-electric actuation can be equivalently taken into account by means of actuating normal forces N_a and actuating bending moments M_a,

$$\delta W_S = \int_0^L (A_{11}\varepsilon - N_a)\,\delta\varepsilon + (D_{11}K - M_a)\,\delta K\,dx. \tag{37}$$

6 Closed Loop Control Algorithm

The realisation of the piezo actuated robot arm is shown in Figure 4. For a patch i, the actuating piezo moment is constant, represented by a constant M_a^i of Eq. (37). Due to the fact that the actuated span of the beam is smaller than the total length of the beam, the feed-forward (ff) piezo moment is increased by a constant factor k_j,

$$M_{a,j}^{\mathrm{ff},i} = k_j\, M_{a,j}^i, \quad k_j = \frac{L_j}{L_{piezo,j}} = \frac{L}{3l_p}. \tag{38}$$

The index j denotes the number of the robot arm $j = 1$ or $j = 2$. While other weighting factors are possible, in the present case a larger number of patches leads to convergence of the solution towards the solution with shaped patches. Alternatively, optimal weighting factors could be computed in order to eliminate vibrations at certain positions or in order to minimize the deformation in the beam, see Nader et al. [7].

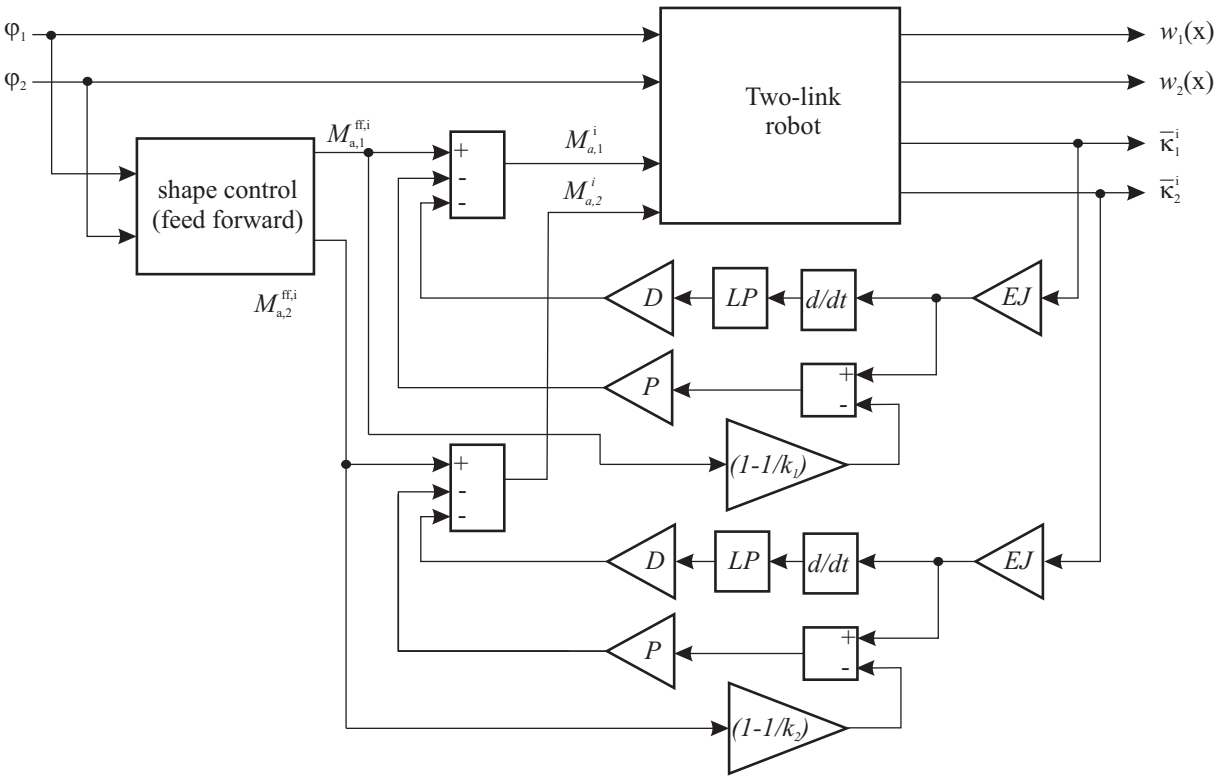

Figure 6: Shape control

The basic strategy of the closed loop controller is sketched in Figure 6. The input of the feed-forward controller is given by the relative joint angles φ_1 and φ_2 of the two robot arms. In a feed-forward controller, the estimated necessary actuating moment $M_{a,j}^{\mathrm{ff},i}$ according to Eq. (38) is applied to the patches. In the feedback controller, the average curvature κ_j^i is measured in each patch i of the robot arm j by means of sensor patches, see Figure 4. The average curvature times patch length also represents the relative angle between the right and left end of the patch. The error of the prescribed average curvature e_κ is given as

$$e_\kappa = \bar{\kappa}_j^i - M_{a,j}^{\mathrm{ff},i}\frac{1 - 1/k_j}{D_{11}}. \tag{39}$$

and is controlled by a slightly modified PD-control law. In order to avoid the differentiation of measured accelerations $\ddot{\varphi}$, the feed-forward actuating moment $M_{a,j}^{\mathrm{ff},i}$ is not included in the differential part of the controller, see Figure 6. Additionally, a low pass filter (LP) is added after differentiation of the error of the prescribed average curvature. The total feedback controlled actuating moment can be written as

$$M_{a,j}^{i} = M_{a,j}^{\mathrm{ff},i} - PD_{11}e_{\kappa} - D\left(D_{11}\,\mathrm{LP}\left(\dot{\bar{\kappa}}\right)\right). \tag{40}$$

7 Numerical Example

As a numerical example, the two-link robot of figure 2, is considered. The material parameters of the two arms with equal dimensions are length $L_1 = L_2 = 0.5$m, rectangular cross section with height $h = 0.01$m, width $b = 0.02$m, density $\rho = 2700\mathrm{kg/m}^3$, Young's modulus $E = 7e10\mathrm{N/m}^2$ and a tip-mass of 1kg. The material is assumed to be linear elastic. The effect of gravity is not considered in this example. It is furthermore assumed that the patches do not influence the bending stiffness $D_{11} = E\frac{bh^3}{12}$ The two links are driven by means of two drives in the hinges of the links. The angle in the hinges is assumed to exactly follow the prescribed angle, thus neglecting effects of an electrical drive or of the gears. The prescribed angles in the two hinges follow the function, see Figure 7,

$$\theta_1 = \theta_2 = 10At^3 - 15At^4 + 6At^5 \quad \text{for} \quad t < 1 \quad \text{and} \quad \theta_1 = \theta_2 = A = \pi/2 \quad \text{for} \quad t \geq 1 \tag{41}$$

which corresponds to a smooth function for the angular acceleration in the hinge and therefore results in a

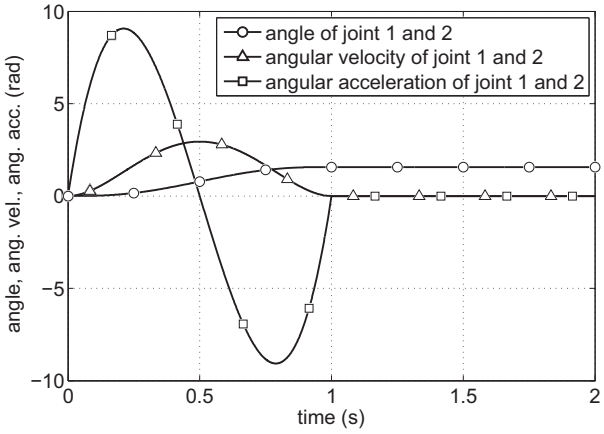

Figure 7: Prescribed angles in joints of two-link robot.

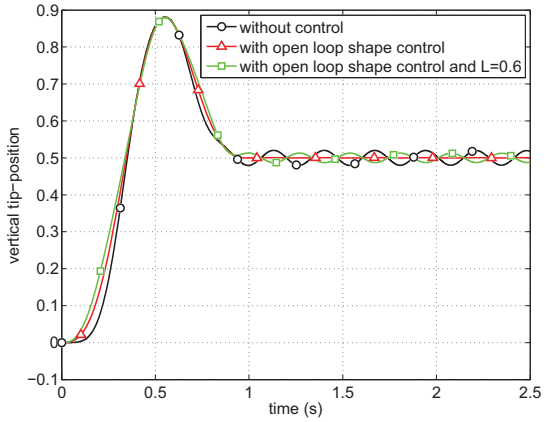

Figure 8: Comparison of vertical tip displacement of the robot without and with piezo-actuated shape control.

smooth motion of the robot. This is a common trajectory for industrial robots. Each arm contains three piezo patches according to Figure 4. The dimensions of the patches are $l_p = 0.1$m and $l_s = 0.05$m resulting in the weighting factor for the shape control $k_1 = k_2 = 10/6$, see Eq. (38). The mechanical system is idealized and does not include any damping.

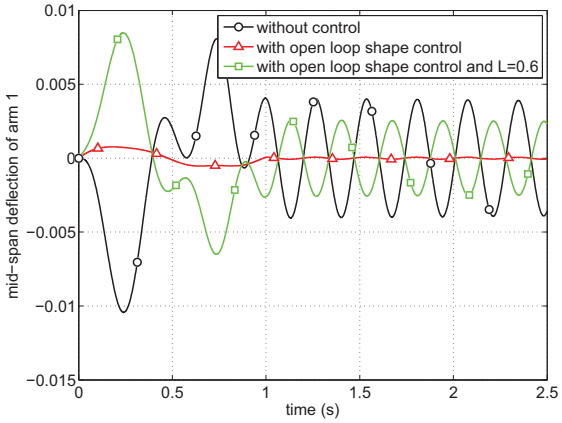

Figure 9: Comparison of the mid-span deflection of arm 1 without and with piezo-actuated shape control.

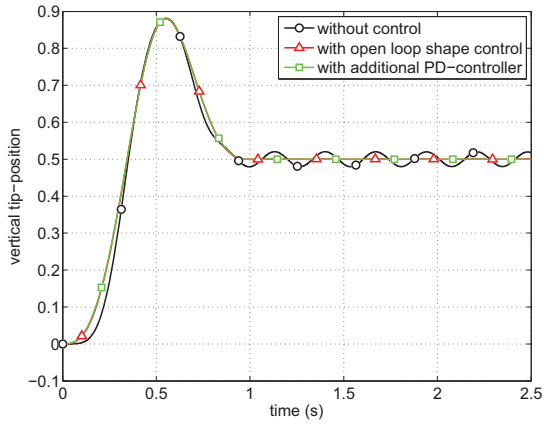

Figure 10: Comparison of vertical tip displacement of the robot without control, with open loop control and with feedback control.

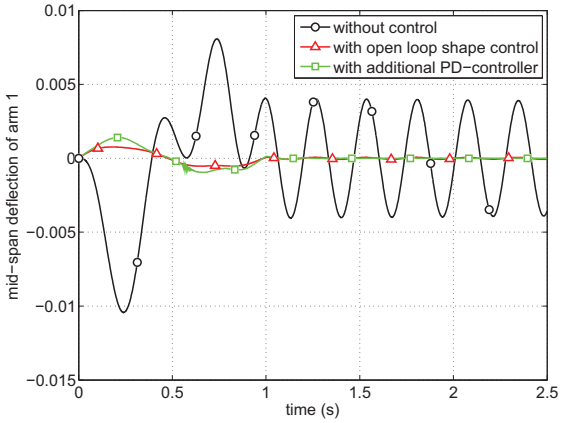

Figure 11: Comparison of the mid-span deflection of arm 1 without control, with open loop control and with feedback control.

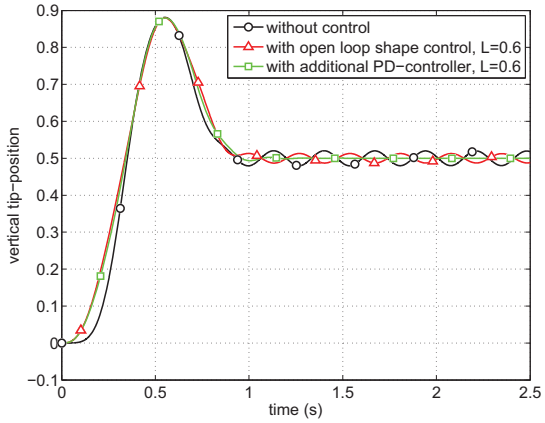

Figure 12: Comparison of vertical tip displacement of the robot without control, with open loop control and with feedback control, using a wrong length of $L = 0.6$m in the control algorithm.

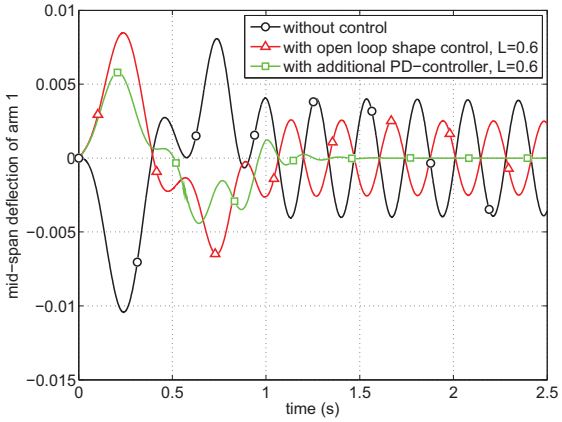

Figure 13: Comparison of the mid-span deflection of arm 1 without control, with open loop control and with feedback control, using a wrong length of $L = 0.6$m in the control algorithm.

As a first investigation, the motion with and without shape control by means of piezo-electric actuation is compared. Figure 8 shows the tip displacement in vertical (y) direction. The final displacement shall be 0.5m. Without control, a significant oscillation of approximately 40mm amplitude remains in the tip deflection in the case without control. In the case with open loop (feed-forward) shape control, the oscillations are not visible in the plot and have about 0.7mm amplitude. In the case of shape control, but with a change of the geometrical parameters to $L = 0.6$ in the feed-forward algorithm, the error in the tip position again becomes approximately 26mm in amplitude. Figure 9 shows the same comparison for the mid-span deflection of the first robot arm.

In the second investigation, the feedback controller is activated with control parameters $P = 1$ and $D = 0.1$. Figures 10 and 11 show the vertical tip position and the mid-span deflection of robot arm 1, respectively. In comparison with the open loop case, the remaining oscillations after the movement of the robot can be fully damped out. However, during the motion, some of the oscillations remain. It is known from the control of piezo-actuated beams, that in some points the deflection and rotation of the cross-section of the beam can be eliminated, depending on the placement and the number of patches. In the current case, the actuation of the patches is purely following the computed distributed bending moment, which is discretized in the mid-point of each patch. Otherwise, the tip deflection could be even eliminated during the whole maneuver with a minimum of two patches per beam and assuming that all system parameters are known.

In the third study, the feedback controller is tested with a disturbance of the geometrical parameters. Thus, the length of both robot arms is set to 0.6m in the feed-forward control algorithm. Figures 12 and 13 show the vertical tip position and the mid-span deflection of robot arm 1 for the case without control, with feed-forward control and with the closed loop control algorithm as given in Eq. (40). This study shows that the feedback controller is able to react to large disturbances of the system. Knowing that the mechanical damping of the real system will further damp oscillations, it can be estimated that the real system might contain even less oscillations.

8 Conclusions

A solution for the shape control problem of an idealized flexible two-link robot has been derived, which fully eliminates the vibrations in the moving robot arms. A numerical model has been set up for the realizable piezo actuated two-link robot, which is able to include geometric imperfections. The numerical example shows that it is possible to significantly reduce the flexible vibrations with the help of feed-forward shape control, if the system parameters are well known. In the case of imperfections, caused by patched shape control and geometric imperfections, an additional feedback control could be implemented, which reduces vibrations significantly. With the implementation of the numerical simulation code it is possible to perform parameter studies in order to find a reasonable configuration for an experimental setup of the piezo actuated robot.

9 Acknowledgments

The support of the present work by the Linz Center of Mechatronics (LCM) and the Austrian Center of Competence in Mechatronics (ACCM) is gratefully acknowledged.

10 References

[1] Sunar, M. and Rao, S.S.: *Recent advances in sensing and control of flexible structures via piezoelectric materials technology*, Applied Mechanics Reviews, 52 (1999), 1–16.

[2] Irschik, H.: *A review on static and dynamic shape control of structures by piezoelectric actuation*, Engineering Structures, 24 (2002), 5–11.

[3] Irschik, H., Nader, M., Zehetner, C.: *Exact cancellation of vibrations in elastic structures performing large rigid body motions*: Proceedings of the Tenth International Congress on Sound and Vibration (Stockholm, 2003, ed. Nilsson A and Boden Hans), 7 (2003), 3487–3498.

[4] Irschik, H., Pichler, U., Nader, M., Zehetner, C.: *Deformation Compensation in Elastic Solids and Structures Performing Rigid-Body Motions*: Advanced Dynamics and Control of Structures and Machines, (CISM,Udine, ed. H. Irschik and K. Schlacher), CISM Courses and Lectures No. 444 (2004), 53–63.

[5] Zehetner, C. and Irschik, H.: *Displacement compensation of beam vibrations caused by rigid-body motions*, Smart Materials and Structures, 14 (2005), 862–868.

[6] Krommer, M. and Irschik, H.: *Sensor and actuator design for displacement control of continuous systems*, Smart Structures and Systems, 3 (2007), 147–172.

[7] Nader, M., Kaltenbacher, M., Krommer, M., von Garssen, H.-G., Lerch, R.: *Active vibration control of a slender cantilever using distributed piezoelectric patches*: Proceedings of The Thirteenth International Congress on Sound and Vibration (ICSV13), Vienna (2006).

[8] Gerstmayr, J. and Irschik, H.: *On the correct representation of bending and axial deformation in the absolute nodal coordinate formulation with an elastic line approach*, Journal of Sound and Vibration, 318 (2008), 461–487.

[9] Gerstmayr, J., Matikainen, M.K., Mikkola, A.M.: *A geometrically exact beam element based on the absolute nodal coordinate formulation*, Journal of Multibody System Dynamics, 20 (2008), 359–384.

[10] Shabana, A. A.: *Dynamics of Multibody Systems* (2nd edition): Cambridge University Press, 1998.